Hindawi
Mathematical Problems in Engineering
Volume 2020, Article ID 5695917, 13 pages
https://doi.org/10.1155/2020/5695917

Research Article

Multiobjective Particle Swarm Optimization for Microgrids Pareto Optimization Dispatch

Qian Zhang,[1,2] **Jinjin Ding**,[3] **Weixiang Shen**,[4] **Jinhui Ma**,[5] **and Guoli Li**[2]

[1]*Department of Electrical Engineering and Automation, Anhui University, Hefei 230039, China*
[2]*Engineering Research Centre of Power Quality, Ministry of Education, Anhui University, Hefei 230039, China*
[3]*Anhui Electric Power Science Research Institute, Hefei 230601, China*
[4]*Electrical Engineering in the Faculty of Science, Engineering, and Technology, Swinburne University of Technology, Melbourne 3059, Australia*
[5]*State Grid Anhui Electric Power Co. Ltd., Hefei 230061, China*

Correspondence should be addressed to Qian Zhang; qianzh@ahu.edu.cn

Received 15 August 2019; Revised 8 December 2019; Accepted 30 January 2020; Published 25 March 2020

Academic Editor: Yang Li

Multiobjective optimization (MOO) dispatch for microgrids (MGs) can achieve many benefits, such as minimized operation cost, greenhouse gas emission reduction, and enhanced reliability of service. In this paper, a MG with the PV-battery-diesel system is introduced to establish its characteristic and economic models. Based on the models and three objectives, the constrained MOO problem is formulated. Then, an advanced multiobjective particle swarm optimization (MOPSO) algorithm is proposed to obtain Pareto optimization dispatch for MGs. The combination of archive maintenance and Pareto selection enables the MOPSO algorithm to maintain enough nondominated solutions and seek Pareto frontiers. The final trade-off solutions are decided based on the fuzzy set. The benchmark function tests and simulation results demonstrate that the proposed MOPSO algorithm has better searching ability than nondominated sorting genetic algorithm-II (NSGA-II), which is widely used in generation dispatch for MGs. The proposed method can efficiently offer more Pareto solutions and find a trade-off one to simultaneously achieve three benefits: minimized operation cost, reduced environmental cost, and maximized reliability of service.

1. Introduction

The increasing concerns over environment have led to a growing demand for renewable energy (RE). More and more presence of RE generations achieves the benefits of greenhouse gas emission reduction and diversity of supply. Due to the intermittent nature of RE, the high penetration of RE generation into power grids has brought challenges to the management of power networks [1–3].

The implementation of multiobjective optimization (MOO) dispatch for microgrids (MGs), which consist of distributed generations (DGs), load systems, storages, and communication systems, can help maximize the benefits while mitigating the negative impacts of DGs on power grids. The MG can operate in both islanded [4–6] and grid-connected modes [7–11]. It is able to improve the stability and reliability of power supply in factory [8], residential districts [9–11], and military zone [12].

The management goal of the MG is not only to satisfy the basic demand of power supply but also to utilize DGs efficiently to improve economic efficiency and environmental protection. There are many approaches to optimize the MG operation. They are generally divided into single objective optimization (SOO) approaches [11, 13–16] and MOO approaches [17–31]. One certain object is concerned though the SOO method, such as energy cost [13, 14]and quality of service [16]. In [11], a hybrid price-based demand response (HPDR) is proposed, in which the MG profit is maximized as a single-objective function. However, the SOO approaches ignore certain benefits, which may be acceptable in some situations. The better solution can be achieved by the MOO approaches for more comprehensive consideration.

The MOO provides many alternative solutions with conflicting nature of different objectives for a decision maker. Weighted sum mode [18] is commonly used to deal with the relationship of different objectives. In [32], the cost of power system operation is formulated as the sum of three parts. It fails to provide an alternative solution of two conflicting objectives. In practice, there are many naturally conflicting goals in the application of MG: minimize the operation cost, maximize the user's comfort, minimize the greenhouse gas emission, minimize the risk, maximize the electricity generation capacity, and minimize the power system losses. A trade-off is unavoidable between these naturally conflicting objectives. Many other methods are introduced to handle differences between the optimal values of various objectives. Fuzzy logic algorithms are proposed to perform social criteria technique in [5, 19, 20]. A modified multiobjective hybrid big Bang-Big Crunch algorithm is employed to cope with the objective functions of voltage overshoot, undershoot, rise time, settling time, and integral time absolute error in [21]. A mixed integer linear programming (MILP) is applied in [22].

Besides these aforementioned methods, the Pareto solution is widely considered as an efficient way to trade-off between the naturally different objectives. The Pareto frontier of the MOO dispatch for the MG system is calculated using various meta-heuristic algorithms [24–31]. The weighted factor as a tuning operator to illustrate the preferences has been modified systematically to obtain the Pareto frontiers. In [26], a technoeconomic approach based on nondominated sorting genetic algorithm-II (NSGA-II) for the MOO is proposed to the design of the photovoltaic-wind hybrid system. NSGA-II is also utilized to the calculation of Pareto optimal fronts in [27].

The traditional PSO shows promising performance on single-objective, nonlinear optimization and gains popularity in the optimal operation of MG. However, it is hard to deal with the multiobjects. The chaos optimization algorithm is introduced to the particle initialization in [20, 23]. This amelioration is useful to discrete space optimization. In [24], a fuzzy self-adaptive particle swarm optimization algorithm is proposed and implemented to dispatch the generations in a typical microgrid considering economy and emission as competitive objectives. Furthermore, an efficient decision-making approach, which adopts the fuzzy adaptive particle swarm optimization algorithm, is suggested to find the best compromise strategy of MG energy management in [25]. Three objective functions, namely, annualized cost of the system, loss of load expected, and loss of energy expected, are considered in [29]. The archiving mechanism is introduced to deal with the multiobjects obtaining a kind of MOPSO. In [30], this algorithm is applied to the optimization of a hybrid wind-PV-battery system for reducing cost and increasing reliability. But it fails to provide an efficient way to the selection and maintenance of the nondominate solutions. In our research, we proposed the external archiving mechanism, in which the maintenance procedure and global best particle selection are improved.

This paper contents are as follows. In Section 2, we build the components and economic models for the illustrated MG system on the basis of optimization dispatch. In Section 3, the MOO problem is proposed with three objects and several constraints for the MG optimization dispatch. In Section 4, an advanced MOPSO algorithm is constructed for the Pareto frontier calculation of the obtained constrained MOO problem after the benchmark function test. In Section 5, the Pareto frontiers and final trade-off solutions are obtained. As conclusion in Section 6, the simulation results demonstrate the proposed modelling method is able to describe the dispatch problem of MG. Besides, the advanced MOPSO has better searching ability than the traditional NSGA-II in Pareto frontier distribution and running time for the MG system under investigation in this study.

2. Modelling of PV-Battery-Diesel MG System

The MG in this study is located in Anhui University, Hefei, Anhui, China, as shown in Figure 1. It is the MG with the PV-diesel-battery system, which includes 400 V/100 kW MG and 400 V/20 kW MG. The MG mainly consists of the PV power system, the diesel generating unit, and the lithium ion (Li ion) battery pack as energy storage. The 400 V/100 kW MG is selected in our simulation and analysis. On the basis of generation dispatch, we will build the characteristic and economic models of the components in the selected MG. Then, the MOO including two objectives and three objectives are carried out under different scenarios.

2.1. Model of PV Array. In the simplified PV steady-state power output model [31], the PV output is only related to solar radiation and ambient temperature:

$$P_{pv}(t) = f_{pv} P_{\mathrm{STC}} \frac{G(t)}{G_{\mathrm{STC}}} \left(1 + k_{pv}\left(T(t) - T_{\mathrm{STC}}\right)\right),$$

$$T(t) = T_{\mathrm{air}}(t) + 0.0138\left[1 + 0.031 T_{\mathrm{air}}(t)\right]\left(1 - 0.042 V_w\right) G(t),$$

$$T_{\mathrm{air}}(t) = 0.5\left[\left(T_{\max} + T_{\min}\right) + \left(T_{\max} - T_{\min}\right)\sin\left(\frac{2\pi\left(t - t_p\right)}{24}\right)\right]. \tag{1}$$

The value of k_{pv} is −0.45% (°C), and the value of T_{STC} is 25°C.

2.2. Model of Diesel Generator. The fuel consumption cost of the diesel generator is mainly related to its output power [33]. It can be expressed by a quadratic polynomial as follows:

$$C_{\mathrm{DE}} = a P_{\mathrm{DE}}^2 + b P_{\mathrm{DE}} + c, \tag{2}$$

where a, b, and c are related to the specific type of diesel generator.

2.3. Model of Li Ion Battery Pack. The state of charge (SOC), which is an important parameter for the battery management, describes the remaining capacity of the Li ion battery pack [13]. It is defined as

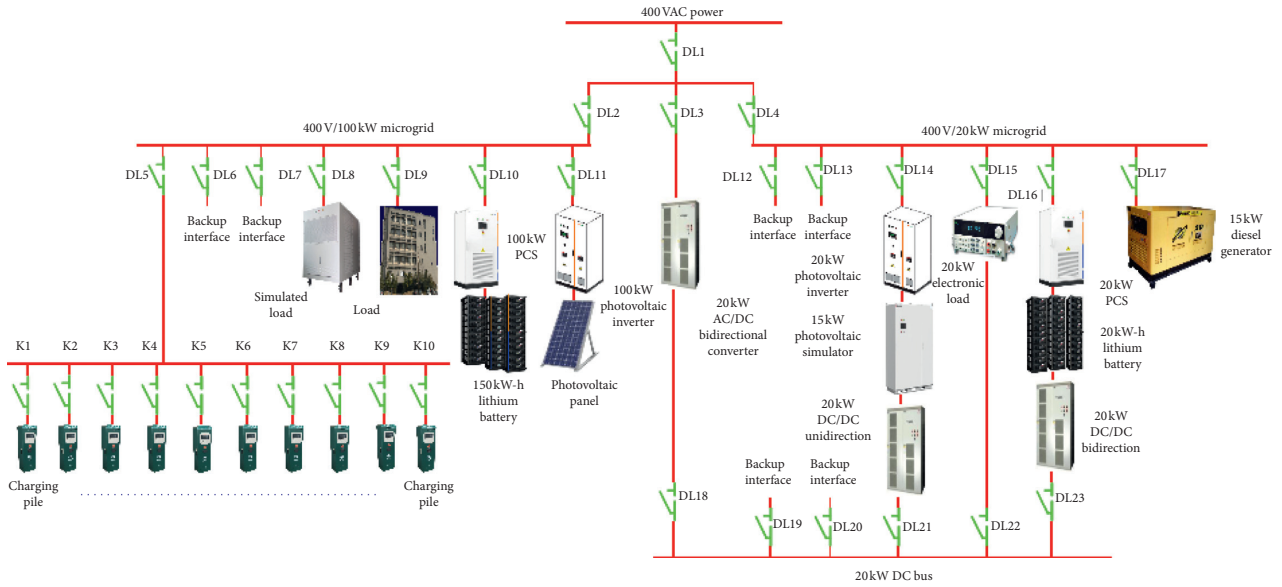

Figure 1: Topological structure diagram of PV-battery-diesel MG system.

$$\mathrm{SOC}(t) = \mathrm{SOC}(t-1) + \frac{\eta_{\mathrm{ch}} I_e(t)}{C_N}, \quad \text{for charge,} \tag{3a}$$

$$\mathrm{SOC}(t) = \mathrm{SOC}(t-1) - \frac{I_e(t)}{C_N \eta_{\mathrm{dis}}}, \quad \text{for discharge,} \tag{3b}$$

$$\begin{aligned} I_e(t) &= \frac{P_{\mathrm{bat}}(t)}{U}, \\ E &= E_0 - K_e \frac{C_{\max}}{C_{\max} - Q_e} + A \exp(-BQ_e), \\ U &= E - I_e(t)R. \end{aligned} \tag{4}$$

2.4. Model of Load considering Plug-In Electric Vehicles. The selected MG mainly supplies a laboratory building, 15 kW power electronic load, and ten electric vehicle (EV) charging piles shown in Figure 1. The daily EV traveling distance approximately satisfies with lognormal distribution, namely, $S \sim \log N(\mu_t, \sigma_t^2)$. Its probability density function $f_s(x)$ is expressed by

$$f_s(x) = \frac{1}{x} \frac{1}{\sigma_s \sqrt{2\pi}} \exp\left(-\frac{(\ln x - \mu_s)^2}{2\sigma_s^2} \right). \tag{5}$$

Thus, the SOC of the EV can be obtained from the daily traveling distance S, which lead to the charging duration as

$$\begin{aligned} T_c &= \frac{\mathrm{SW}_{100}}{100 P_c \eta_{C\_\mathrm{EV}}}, \\ P_{\mathrm{EV}i} &= \frac{\mathrm{SW}_{100}}{100}. \end{aligned} \tag{6}$$

The daily load of a certain number of the EV charging is obtained by the Monte Carlo method:

$$P_{\mathrm{EVload}}(t) = \sum_{i=1}^{N_{\mathrm{EV}}} P_{\mathrm{EV}i}. \tag{7}$$

3. Problem Formulation

3.1. The First Objective Function: Operation Cost. The optimization objective F_1 contains energy consumption cost C_{dg}, the operation management cost C_{om}, the depreciation cost of battery C_{bd}, and the energy interaction cost between the grid and MG C_{grid}. MG absorbed power from the power grid with the purchase price and output power to the power grid with the electricity price:

$$\min F_1 = \sum_{t=1}^{24} \left(C_{\mathrm{dg}} + C_{\mathrm{om}} + C_{\mathrm{grid}} + C_{\mathrm{bd}} \right), \tag{8}$$

$$C_{\mathrm{dg}} = \sum_{i=1}^{N_{\mathrm{DG}}} C_{fi} \cdot P_i(t), \tag{9}$$

$$C_{\mathrm{om}} = \sum_{i=1}^{N_{\mathrm{DG}}} K_i \cdot P_i(t), \tag{10}$$

$$C_{\mathrm{grid}}\left(P_{\mathrm{grid}}(t) \right) = \begin{cases} c_{\mathrm{p}}(t) P_{\mathrm{grid}}(t), & P_{\mathrm{grid}}(t) \geq 0, \\ c_{\mathrm{s}}(t) P_{\mathrm{grid}}(t), & P_{\mathrm{grid}}(t) < 0, \end{cases} \tag{11}$$

$$C_{\mathrm{bd}} = \sum_{i=1}^{N} C_{\mathrm{bw}} \cdot P_i(t), \tag{12}$$

where N_{DG} is a total number of DGs, $P_i(t)$ is the energy output of the i_{th} DG, and $P_{\mathrm{grid}}(t)$ is the electricity exchange between the MG and power grid. C_{fi}, K_i, and C_{bw} are the ECC, OMC, and BDC coefficients of the i_{th} DG. $c_p(t)$ is the electricity purchasing price when the MG absorbs energy

from the power grid, which varies with the peak and valley periods. $c_s(t)$ is the electricity selling price when the MG delivers power to the power grid, which is higher than the electricity purchasing price because of the subsidization from the government. These coefficients of the studied MG are summarized in Tables 1 and 2.

3.2. The Second Objective Function: Environmental Cost. The environmental cost is as important as the economic one. It can be divided into two parts [34]. The first component is the environmental value of power generation emissions, which represents the environmental influence in the operation of MG. The other part is the pollution fine for the emissions, which determined by the jurisdiction. Therefore, the environmental protective cost is considered in the dispatch model, which is defined as follows and in Table 3:

$$\min F_2 = \sum_{t=1}^{24} \sum_{i=1}^{N_P} \left(\left(\alpha_i(t) + \beta_i(t) \right) Q_i(t) \right). \tag{13}$$

3.3. The Third Objective Function: Loss of Load Probability. Reliability is one of the important factors in the MG planning and operation. In [34], the adequacy of power to meet load demand is expressed by loss of load probability (LOLP). In this study, the LOLP is only considered in the islanded operation mode.

For the convenience of calculation, an auxiliary quantity—Boolean quantity, is defined, that is,

$$H_{\mathrm{LOLP}(t)} = \begin{cases} 0, & \Delta_t \geq 0, \\ 1, & \Delta_t < 0, \end{cases} \tag{14}$$

where $H_{\mathrm{LOLP}(t)}$ is a Boolean and Δ_t is the quantity of power imbalance at time t. The LOLP can be expressed as

$$\mathrm{LOLP} = -H_{\mathrm{LOLP}(t)} \cdot \frac{\left(P_{\mathrm{tot}} - P_{\mathrm{load}} \right)}{P_{\mathrm{tot}}}. \tag{15}$$

The third optimization objective F_3 of the MG is defined as

$$\min F_3 = \mathrm{LOLP}. \tag{16}$$

3.4. Constraints of MG. The natural power generation constraints impact the flexibility of MG system and participate in generation units on reserve and energy markets [35]. The constraints in this study are listed as follows:

(1) Power balance constraints:

$$P_{\mathrm{load}}(t) = P_{\mathrm{PV}}(t) + P_{\mathrm{gen}}(t) + P_{\mathrm{bat}}(t) + P_{\mathrm{grid}}(t). \tag{17}$$

(2) DG capacity constraints:

$$P_{i,\min} \leq P_i(t) \leq P_{i,\max}. \tag{18}$$

(3) Transmission capacity constraints:

$$P_{\mathrm{grid},\min} \leq P_{\mathrm{grid}}(t) \leq P_{\mathrm{grid},\max}. \tag{19}$$

Table 1: Maximum power and ECC, OMC, and BDC coefficients.

Electricity price	Peak period (\$/kW) (8 : 00–22 : 00)	Valley period (\$/kW h) (22 : 00-next 8 : 00)
$c_p(t)$	0.09297	0.04924
$c_s(t)$	0.1562	

(4) Capacity constraints of Li ion battery:

$$\mathrm{SOC}_{\min} \leq \mathrm{SOC}(t) \leq \mathrm{SOC}_{\max}. \tag{20}$$

(5) Capacity constraint of service transformer:

$$S_{\mathrm{load}} < \beta \cdot S_N. \tag{21}$$

3.5. Constrained Multiobjective Optimization Problem. The constrained MOO problem deals with the dispatch of the DGs to satisfy the multiple objectives of the MG, limited by the constraints and operating limits. It can be formulated as

$$\begin{aligned} \min \quad & F(x) = \min\left(F_1(x), F_2(x), F_3(x) \right) \\ \text{s.t.} \quad & \text{constraints}\,(17)\text{–}(21). \end{aligned} \tag{22}$$

The objects and constraints are defined as (8)–(22).

4. Pareto Particle Swarm Optimization Algorithm

In recent years, Pareto optimality is applied in engineering and social sciences [36]. It is defined as allocating goods among individuals where no individual can improve its situation without worsening another's. When two or more conflicting objectives are sought to be minimized, there will not be a single solution that is optimal for every objective function; instead, the optimal solution set comprises multiple solutions with a trade-off between the objectives, namely, the Pareto-optimal front.

4.1. Pareto Domination. Let F: $\mathbb{R}^n \longrightarrow \mathbb{R}^m$ be the function that assigns a criteria space point $F(X)$ to each design space point $X \in \Theta \subseteq \mathbb{R}^n$, Θ is the search space, where the vector X is the set of all feasible solutions in $\mathbb{R}^n$, and the objective vector $Y = F(X)$ represents their measured values in $\mathbb{R}^m$. We consider n real parameters and m objectives in a constrained MOO problem to define a Pareto optimal front.

Definition 1. Let a solution vector be X_0, X_0 is said to dominate a particle X_1, if and only if $J(X_0) \leq J(X_1)$. X_0 is said to be Pareto optimal if $\exists X_1$ dominates X_0, $X_1 \succ X_0$.

Definition 2. Pareto optimal set $\mathscr{P}_s$ of all Pareto optimal decision vectors is defined as $\mathscr{P}_s = \{X_0 \in \Theta \mid \exists X_1 \in \Theta, X_1 \succ X_0\}$. All Pareto optimal values corresponding to the decision vectors in $\mathscr{P}_s$ constitute the Pareto optimal front $\mathscr{P}_F$.

Table 2: Electricity purchasing/selling price from/to market.

Types of DGs	Maximum of input/output power (kW)	ECC coefficient ($/kW)	OMC coefficient ($/kW)	BDC coefficient ($/kW)
PV array	115	5703.125	0.009 6	0.020
Diesel generator	15	2500	0.088	0.064
Li ion battery pack	170	440.46875	0.009	0.108
EV charging pile	3×10	520.78125	0.009	0.096

Table 3: Standard coefficients of environmental value and pollution penalty in power industry ($/kg).

Coefficients	SO_2	NO_x	CO_2	CO
Environmental value $\alpha_i(t)$	0.75	1.00	0.002875	0.125
Emission fine $\beta_i(t)$	0.125	0.250	0.00125	0.020

4.2. The Standard PSO. The standard PSO is a kind of the heuristic optimization algorithm, which attracts significant attention since its introduction in 1995.

In the standard PSO algorithm, the i_{th} particle $X_i = \{x_{i1}, \ldots, x_{in}\}$ represented by its position in the n-dimensional space is a potential solution to the problem. Within the search space, the i_{th} particle flies under a velocity $V_i = \{v_{i1}, \ldots, v_{in}\}$. In each flying step, say the t_{th} step, the best position of the i_{th} particle $P\text{best}_i(t)$ is $\{P\text{best}_{i1}(t), \ldots, P\text{best}_{in}(t)\}$, and the best position of the entire swarm $G\text{best}(t)$ is $\{G\text{best}_1(t), \ldots, G\text{best}_n(t)\}$. At the $(t+1)_{\text{th}}$ step, the new position for the i_{th} particle can be determined by

$$\begin{aligned} v_{ij}(t+1) &= w \times v_{ij}(t) + c_1 \times \text{rand1} \times \left[P\text{best}_{ij}(t) - x_{ij}(t)\right] \\ &\quad + c_2 \times \text{rand2} \times \left[G\text{best}_j(t) - x_{ij}(t)\right], \\ x_{ij}(t+1) &= x_{ij}(t) + v_{ij}(t+1), \\ w &= w_{\max} - \frac{w_{\max} - w_{\min}}{T} \times t, \end{aligned} \tag{23}$$

where rand is a uniform random value in the range of [0, 1].

4.3. Advanced MOPSO. To achieve the Pareto front in this constrained MOO problem, there are two critical steps: archive maintenance and Pareto selection. The external archive is used to store some of the nondominated solutions produced in the searching process of the MOO algorithm.

The selection of *G*best is crucial in the PSO algorithm. In the single-objective PSO, all the particles have the same*G*best. Thus, we can choose the best solution of fitness function as *G*best in SOO progress. However, in the MOO problem, several nondominate solutions will be obtained from the whole population in each evolution iteration. The archive maintenance aims to get diversified *G*best, while the best choice of *G*best for each particle helps to improve or maintain the diversity of external archives.

In this paper, the advanced MOPSO with a mixed process of performing external archive maintenance and *G*best selection is proposed. The new nondominated solution becomes a member of the external archives, if it satisfies one of the following three conditions: (i) the new solution dominates some members of the external archive; (ii) the external archive size is less than its maximum size; (iii) the new solution has better density when the external archive already has the maximum size. The Manhattan distance D_{ij} is introduced to describe the distance between two solutions X_i and X_j as

$$D_{ij} = \frac{1}{M} \sum_{k=1}^{M} u_k \left| F_k(X_i) - F_k\left(X_j\right) \right|, \tag{24}$$

$$u_k = u_{k-1} \times \left(\frac{\max F_k}{\max F_{k-1}} \right). \tag{25}$$

The combination procedure of archive maintenance and *G*best selection is analysed in three different conditions. For a new nondominate solution X_i, the following conditions apply:

(i) The first possibility is X_i dominates some solutions in external archive N_p, then X_i takes the place of dominated solutions and will be chosen as *G*best.

(ii) Otherwise, if $N_a = \overline{N}$, where N_a is the size of current external archive while $\overline{N}$ is its maximum size, remove a best member X_l with minimum crowding measure under (24) and (25). If $X_l \neq X_k$, substitute X_l for the global best position of all particles in N_a.

(iii) If $N_a < \overline{N}$,

  (a) For all the $X_k \in Np$, set $s = \min_{k=1,2,\ldots,Np}\{hp(X_k)\}$.

  (b) $F = \{X_k \in Np \mid hp(X_k) > g\}$, $d = |F|$, g is a constant, and $g \in [0.025N, 0.05N]$. $u = 1$.

  (c) Select a solution $X_k \in F$ with minimum crowding measure fromX_i and replace *G*best as X_i. $F = F \backslash \{X_k\}$, $hp(X_i) = hp(X_i) + 1$, and $u_k = u_{k+1}$.

  (d) If $hp(X_i) < s$ and $u_k < d$, turn to (*c*).
  If $hp(X_i) < s$ and $u_k = d$, turn to (*b*).
  If $hp(X_i) = s$, insert X_i into external archive.
  End if.

The cardinality of the set F is denoted by $|F|$. The flowchart of the advanced MOPSO is demonstrated in Figure 2. The terminating condition in the program is (i) if the maximum number of iterations is meet or (ii) the desired change of fitness function is meet.

4.4. Benchmark Function Test. Three representative benchmark functions associated with their dimensions and

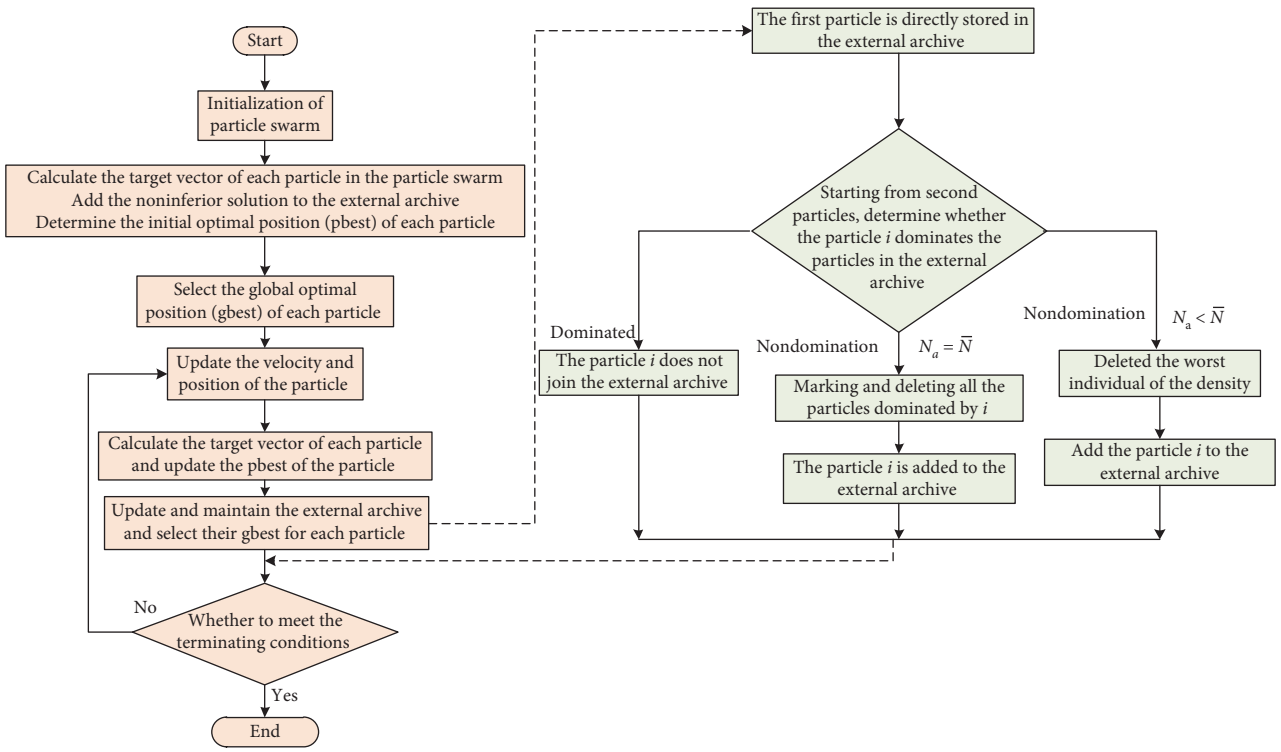

Figure 2: Flowchart of the proposed advanced MOPSO.

bounds of the variables shown in Table 4 are used to test the effectiveness of the advanced MOPSO. The testing results are compared against those obtained by the traditional NSGA-II, which is well known and widely used in the optimization dispatch and energy management of MGs. The spread of the solutions in the nondenominated fronts is measured by the variance of the nearest distance between neighbor solutions [36]. The spacing matric S_p is introduced as a quantitative measure to evaluate the spread of the solutions to the multiobjective algorithm. S_p is defined below.

$$d_i = \min_j\left(D_{ij}\right), \tag{26}$$

$$\overline{d} = \frac{1}{n-1}\sum_{i=1}^{n} d_i, \tag{27}$$

$$S_p = \sqrt{\frac{1}{n-1}\sum_{i=1}^{n}\left(\overline{d} - d_i\right)^2}, \tag{28}$$

where $n$is the number of solutions in Pareto optimization set, D_{ij} is the Manhattan Distance defined in (27) and (28), and $\overline{d}$ represents the average value of all d_i. The values of S_p is lower when the solutions in the Pareto frontier set spread more even.

Based on the prior research [37], the advanced MOPSO is run multiple times for the selection of parameters. Finally, in our test, the parameters in advanced MOPSO are set in Table 5. The parameters of NSGA-II are set following Ref. [38] as follows: population size is 100, maximum iteration is 500, crossover probability is 0.5, and mutation probability is 0.3. The advanced MOPSO and NSGA-II are run independently 200 times under the same conditions.

To display the difference of optimal Pareto frontier between the given method and the real one clearly, the best optimal Pareto frontiers of MOPSO and NSGA-II are shown in Figures 3–5.

Figures 3–5 display that the optimal Pareto frontiers of MOPSO for ZDT1, ZDT2, and ZDT3 are almost same as the real Pareto frontiers. Compared with NSGA-II, MOPSO obtains better solution set in both convergence and diversity. The optimal Pareto frontiers obtained by MOPSO are almost the same with the real Pareto frontiers, which are significantly superior to the traditional NSGA-II in both convergence and diversity. This owes to the combination of the archive maintenance and Pareto selection. The external archive helps to store enough nondominated solutions, and the replacement strategy is able to seek the coincident and continuous dominate solutions. While in NSGA-II and the other optimization algorithms, the possible solutions are less likely to survive when they are crowding in multiobjective dimensions.

For the purpose of further comparison, the worst, best, mean, and standard deviations (Std.) of S_p with MOPSO and NSGA-II for benchmark tests are shown in Table 6. Meantime, the average running times are also listed in Table 6.

The results show that MOPSO has better solutions of S_p and less operating time than the traditional NSGA-II. This

Table 4: Standard test functions.

	Test function	Dimension	Variable bounds	Character of Pareto frontier
ZDT1	$\min f_1(x) = x_1$, $\min f_2(x) = g(x)h(f_1(x), g(x))$, $g(x) = 1 + (9/29)\sum_{i=2}^{30} x_i$, $h(f_1(x), g(x)) = 1 - (f_1(x)/g(x))^{1/2}$	30	[0, 1]	Convex
ZDT2	$\min f_1(x) = x_1$, $\min f_2(x) = g(x)h(f_1(x), g(x))$, $g(x) = 1 + (9/29)\sum_{i=2}^{30} x_i$, $h(f_1(x), g(x)) = 1 - (f_1(x)/g(x))^2$	30	[0, 1]	Nonconvex
ZDT3	$\min f_1(x) = x_1$, $\min f_2(x) = g(x)h(f_1(x), g(x))$, $g(x) = 1 + (9/29)\sum_{i=2}^{30} x_i$ $h(f_1(x), g(x)) = 1 - \sqrt{(f_1(x)/g(x))} - (f_1(x)/g(x))\sin(10\pi f_1(x))$	30	[0, 1]	Convex disconnect

Table 5: Related parameters in advanced MOPSO.

	$w_{\max}$	$w_{\max}$	c_1	c_2	N	N_a
ZDT1	0.4	0.9	2	1	200	80
ZDT2	0.4	0.9	2	2	200	80
ZDT3	0.4	0.9	2	1	200	200

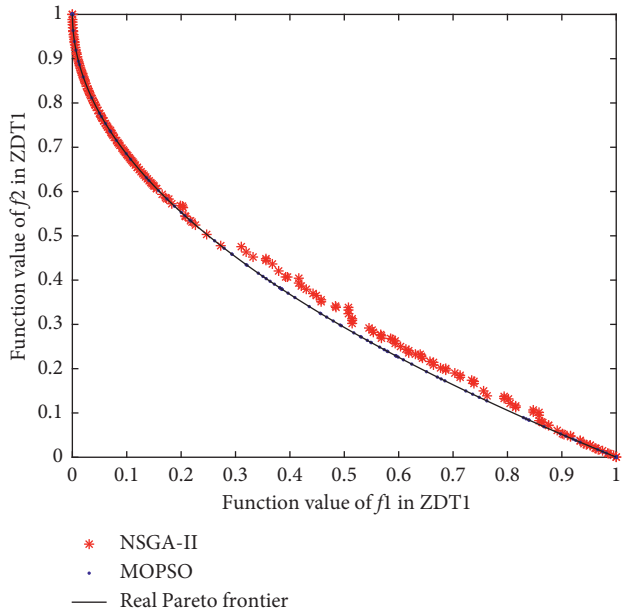

Figure 3: Comparison of real Pareto front and Pareto fronts calculated by MOPSO and NSGA-II for ZDT1.

indicates better performance of the proposed algorithm in the aspect of searching of nondominated front.

5. Experiments and Analysis

The benchmark function tests demonstrate the effectiveness and advantages of the proposed MOPSO algorithm. Then, we apply this method to the constrained MOO problem in the optimization dispatch for the MG with the PV-battery-diesel system. The MG in Figure 1 can operate in both grid-connected and islanded modes (latitude: 31°51′S and longitude: 117°16′W). According to different operation modes and solar radiation intensity, four scenarios are investigated, as shown in Table 7. When the MG works in the grid-connected mode, the

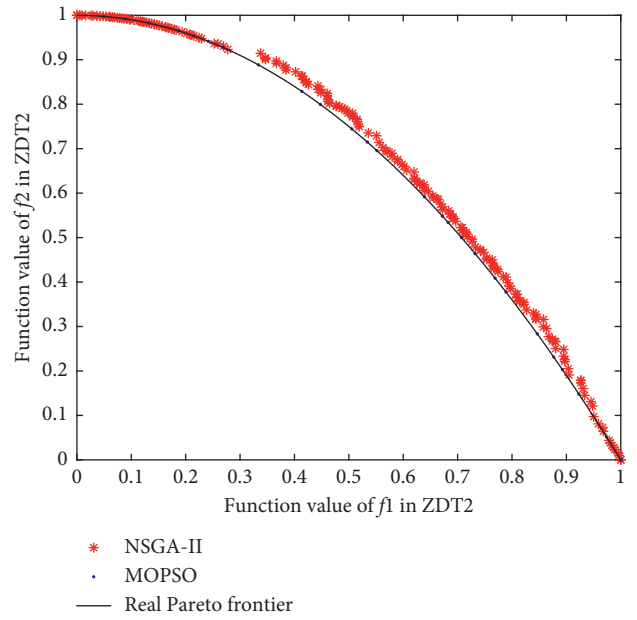

Figure 4: Comparison of real Pareto front and Pareto fronts calculated by MOPSO and NSGA-II for ZDT2.

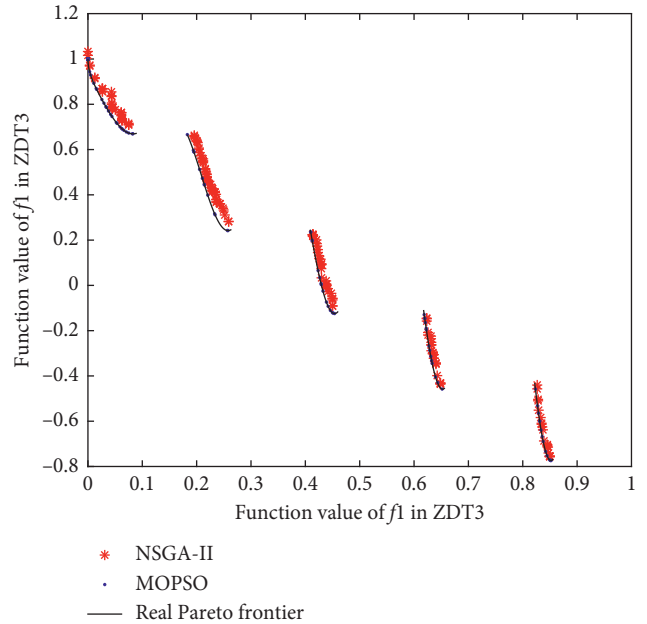

Figure 5: Comparison of real Pareto front and Pareto fronts calculated by MOPSO and NSGA-II for ZDT3.

Table 6: Worst, best, mean, and standard deviations of S_p.

Fun.	Algorithm	Worst	Best	Mean	Std.	Average running time
ZDT1	MOPSO	0.0081	0.0049	0.0069	8.93e – 004	55.2024s
	NSGA-II	0.0106	0.0071	0.0082	0.0021	160.2151s
ZDT2	MOPSO	0.0080	0.0049	0.0062	0.0017	62.8830s
	NSGA-II	0.0082	0.0052	0.0064	0.0019	171.0365s
ZDT3	MOPSO	0.0085	0.0060	00065	5.63e – 004	52.1894s
	NSGA-II	0.0105	0.0067	0.0084	0.0018	163.9019s

Table 7: Four scenarios for optimal dispatch of MG with PV-battery-diesel system.

Optimization scenario	Grid-connected mode	Islanded mode
Strong solar radiation in summer	Scenario 1	Scenario 3
Weak solar radiation in winter	Scenario 2	Scenario 4
A number of objectives	2	3

third objective of the LOLP is neglected, and only the first two objectives are considered in the Scenarios 1 and 2. When the MG works in the islanded mode, three objectives are considered in the Scenarios 3 and 4, as shown in Table 7.

The flexibility of load in the laboratory building varies over one day or one season and has a different value for each time period. In this paper, the flexibility of buildings for various time periods has been extracted as the typical days shown in Figure 6. In winter, a day with weak solar radiation (January 5, 2018) is chosen as Scenarios 2 and 4. When PV power is low, it is important to dispatch the energy from the main grid or other distributed generation. In summer, a day with strong solar radiation (July 28, 2018) is chosen as Scenarios 1 and 3. Under this situation, the PV power and load demand are both high, and the battery management is crucial for the dispatch optimization.

5.1. Pareto Frontiers. Finally, in the experiment, parameters in advanced MOPSO are set as below: $c_1 = c_2 = 2$, linear decreasing inertial weight with $w_{\max} = 0.9$ and $w_{\min} = 0.4$, the population size of swarm $N = 200$, and the maximum number of iteration $T = 600$. With the lowest economic and environmental costs as the objective function when the MG operates in the grid-connected mode under Scenarios 1 and 2, the Pareto frontiers with the two objectives are calculated by using the MOPSO and NSGA-II, and the results are shown in Figures 7 and 8, respectively.

For the constrained MOO problem in the optimization dispatch for the MG, NSGA-II algorithm obtains 14 Pareto solutions with the following spread: (55.3$, 48.5$) and (71.8$, 26.9$). However, the advanced MOPSO algorithm obtains 67 solutions spreading in the range of (54.22$, 48.68$) and (72.29$, 26.03$), as shown in Figure 7. In Figure 8, it is shown that the traditional NSGA-II method only finds 19 solutions in Scenario 2, while the MOPSO

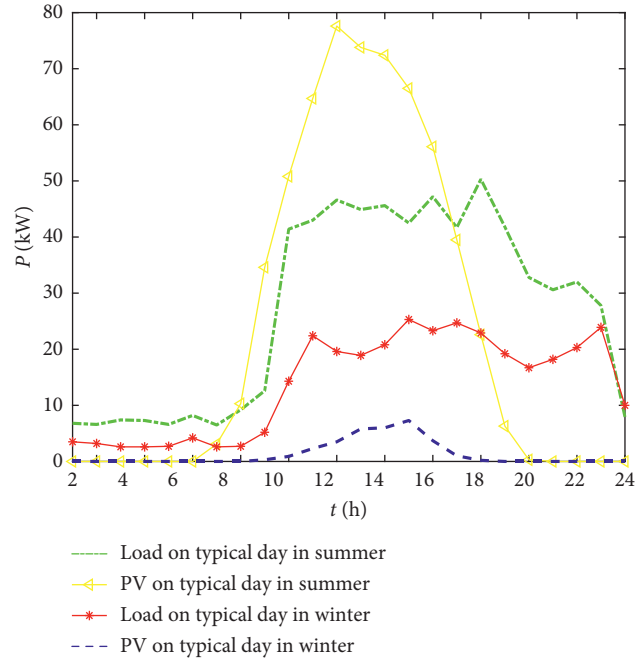

Figure 6: Typical daily load demand and PV output power of MG under strong and weak solar radiation in winter.

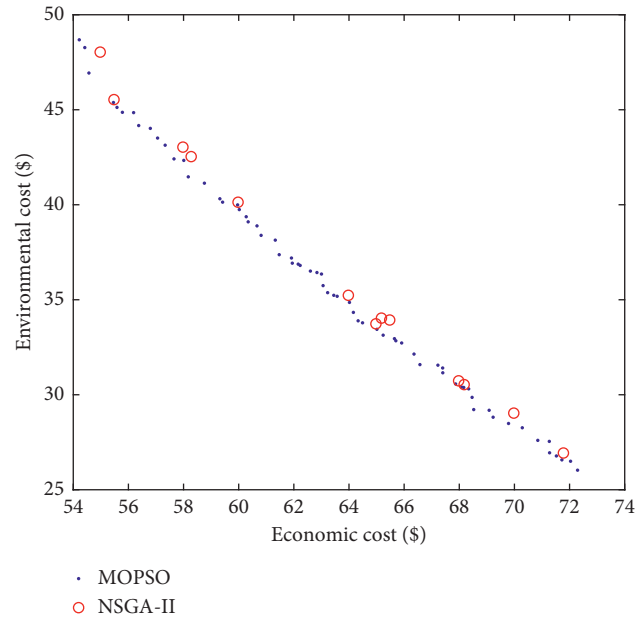

Figure 7: Pareto frontiers of two objectives optimization in Scenario 1.

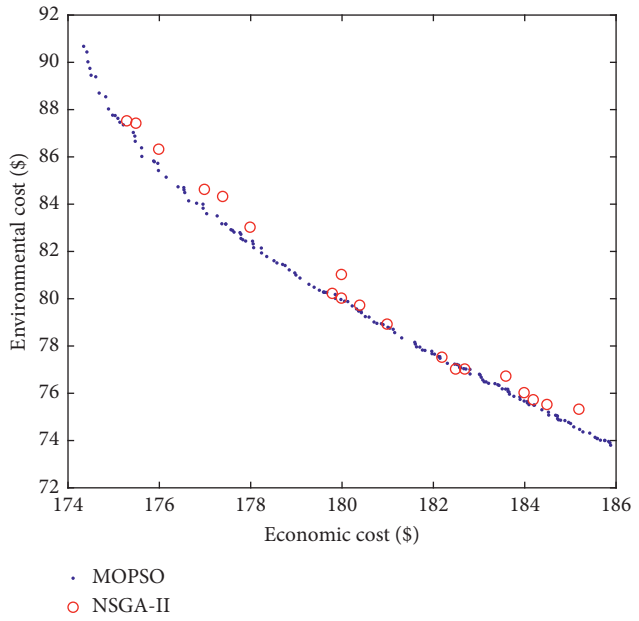

Figure 8: Pareto frontiers of two objectives optimization in Scenario 2.

method gets 118 possible solutions in Pareto frontier sets. The advanced MOPSO algorithm gives a value as low as 174.3$ in economic cost and 73.9$ in environmental cost. For comparison, the traditional NSGA-II method gives a value as low as 175.3$ in economic cost and 75.3$ in environmental cost.

When the MG operates in the islanded mode under Scenarios 3 and 4, there are three objective functions in optimization dispatch. The three objective functions are lowest economic cost, environmental cost, and LOLP. In the islanded mode, the diesel generator starts to work together with the PV power, supplying the load demand and recharging the Li ion battery pack. The Pareto frontiers with three objectives are calculated by using the MOPSO and NSGA-II, and the results are shown in Figures 9 and 10, respectively. There are no comparison results offered by the traditional NSGA-II because it fails to get the Pareto frontiers of the three-object problems. Meantime, the MOPSO provides the Pareto frontiers as shown before. The average running times in the four scenarios are listed below. The superiority of the proposed method is obvious for comparison.

It is demonstrated that the proposed MOPSO algorithm has better performance in variable domains of economic and environmental cost.

5.2. Final Trade-Off Solution. After the obtaining of the Pareto optimal solutions using the proposed methods, it comes to the stage of choosing one best compromise solution for real applications. When the MG works in the grid-connected mode, the fuzzy set [39] is introduced to handle the challenges of inaccurate nature for the MG system. The membership function η is defined below. The solution with the largest membership function is chosen as the final trade-off solution:

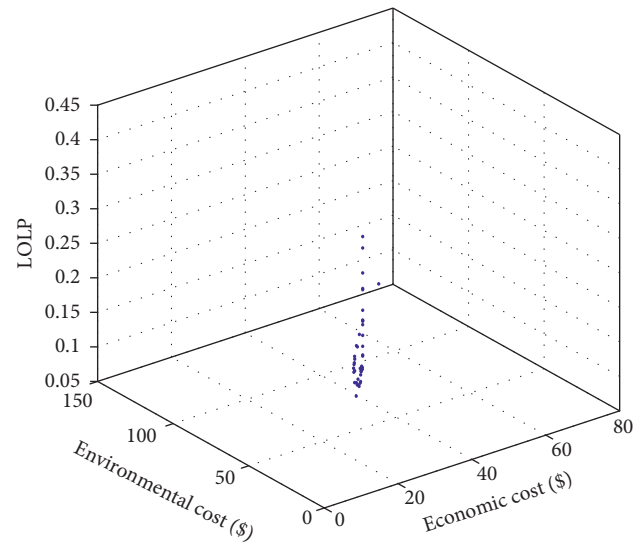

Figure 9: Pareto frontiers of three objectives optimization in Scenario 3.

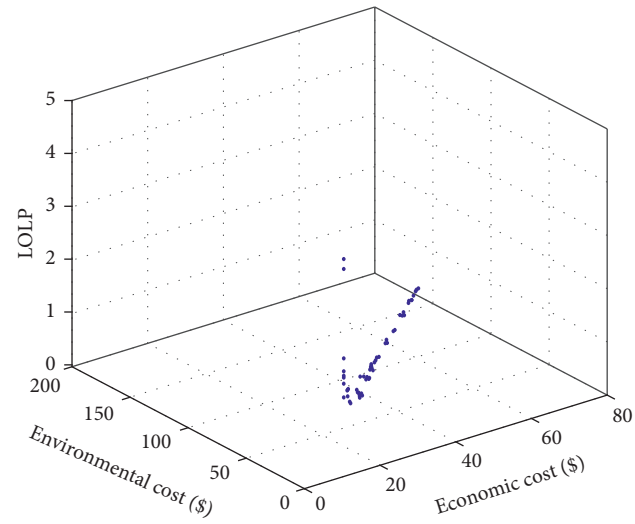

Figure 10: Pareto frontiers of three objectives optimization in Scenario 4.

$$\eta = \frac{1}{M}\sum_{i=1}^{M}\frac{f_{i\max} - f_i}{f_{i\max} - f_{i\min}}. \tag{29}$$

Each nondominated solution is a possible scheduling scheme of the MG. The final trade-off solution is selected according to the membership function formula (26).

The solution with the largest membership can be considered as the final trade-off solution. The optimal dispatch plans of distributed generations and power grid corresponding to this optimal solution are shown in Figures 11 and 12 under Scenarios 1 and 2, respectively. Under Scenario 1, PV output focuses on the daytime period, especially from 9 to 15. Besides satisfying the system load, the excess power from the PV generation is not only charged to the lithium

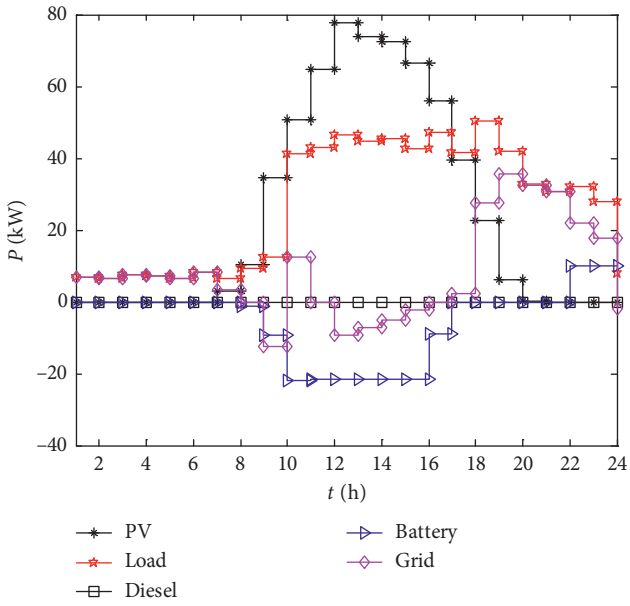

Figure 11: Distributed power and grid output power in Scenario 1.

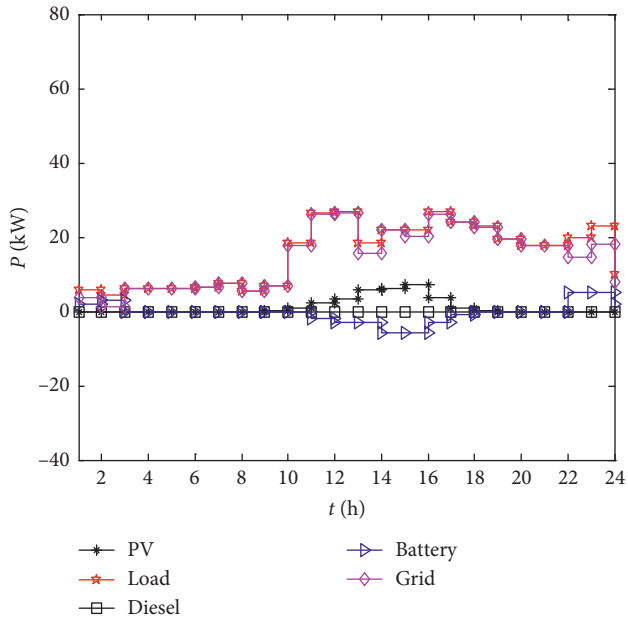

Figure 12: Distributed power and grid output power in Scenario 2.

ion battery but also to the large power grid for the economic benefit.

Under the weak solar radiation in winter, the output of PV power generation is low. The load of the system is mainly provided by the output of the large power grid. In the evening, the load is relatively small, and the lithium ion battery is in the discharge state. The battery subsystem works together with the large power grid to meet the load demand. Under Scenario 2, PV power generation is insufficient to meet the load demand of the system, so the power grid is in the state of power generation. Diesel generators have high economic and environmental costs; thus, it does not work either in Scenario 1 or Scenario 2. The final solution of the proposed Pareto MOO problem using the MOPSO algorithm is reasonable. The economic and environmental costs are listed in Table 8. For comparison, the solutions of NSGA-II under these two scenarios are also listed in the same table. The economic and environmental costs are (58.17$, 42.16$) and (176.64$, 84.14$) in Scenario 1 or Scenario 2 using the MOPSO algorithm, with the comparison of (58.21$, 43.38$) and (177.29$, 84.37$). It is shown that the proposed method is able to obtain better solution in the economic and environmental aspects than the traditional NSGA-II method.

When the MG is operated in an isolated mode, it is critical to consider the probability of load loss of the system. In these situations, the trade-off solution is chosen as the one of the minimum load loss probabilities. Although the corresponding MG system runs the maximum economic and environmental costs under the minimum load loss probability, the primary goal of the operation of the MG system should be to meet as many load requirements as possible, so the trade-off solution of the minimum load loss probability is still selected as the three target optimization operation of the MG system.

Under the Scenario 3, the optimal dispatch plans of distribution generations are shown in Figure 13. The diesel generator is used to meet the load demands in the islanded mode of MG. In summer under strong solar radiation, PV can provide the load in day time. Meanwhile, the lithium ion battery package charges power in this period. During 17 : 00–19 : 00, the diesel plays as a supplementary role in energy supply, and lithium ion battery package works in discharge state as well. In the evening, the output power of lithium ion battery package reaches its maximum. The optimized economic, environmental costs, and LOLP is (105.61$, 71.05$, 0.02).

Under the Scenario 4, the solar radiation is weak in the winter typical daily. The diesel is the main energy supply in the islanded MG system in day time, while lithium ion battery package discharges during 19 : 00–22 : 00. The optimal dispatch plan of the MG is illustrated in Figure 14, and the optimized economic, environmental costs, and LOLP is (188.34$, 142.95$, 0.01). Because of the long-term running of diesel, the environmental cost is highest among the four scenarios. On the contrary, with lower dependence on PV, the LOLP is down from 0.02 to 0.01.

There is no comparison of three objectives optimization between NSGA-II, as it fails to find the Pareto solution. The economic and environmental costs during one day corresponding to the extreme solution and the trade-off solution under different optimization scenarios are shown in Table 8. The average running times are listed as well.

From the simulation results presented in Table 8, the numerical results are better than the comparison algorithm but not by much. This is mainly because the simulation results are obtained for a small-scale MG system, and the cost savings are only for 1 day. Compared with NSGA-II, the economic and environmental costs can be further reduced. In the meantime, the running time of the proposed method is reduced to nearly 30% of the NSGA-II. It is beyond the request of day-ahead Pareto optimization dispatch. Thus, it is demonstrated that the proposed optimal method has superiority in practice.

Table 8: Optimization results in different scenarios.

Final solution		Economic cost ($)	Environmental cost ($)	Loss of load probability	Average running time (second)
Scenario 1	MOPSO	58.17	42.16	—	48.1159
	NSGA-II	58.21	43.38	—	122.6793
Scenario 2	MOPSO	176.64	84.14	—	48.5965
	NSGA-II	177.29	84.37	—	124.6548
Scenario 3	MOPSO	105.61	71.05	0.02	54.1296
	NSGA-II		Failed		—
Scenario 4	MOPSO	188.34	142.95	0.01	55.6132
	NSGA-II		Failed		—

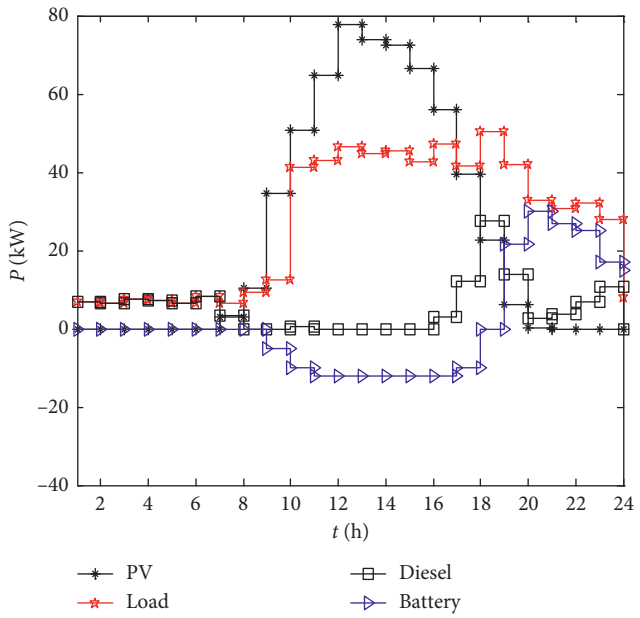

Figure 13: Distributed power and grid output power in Scenario 3.

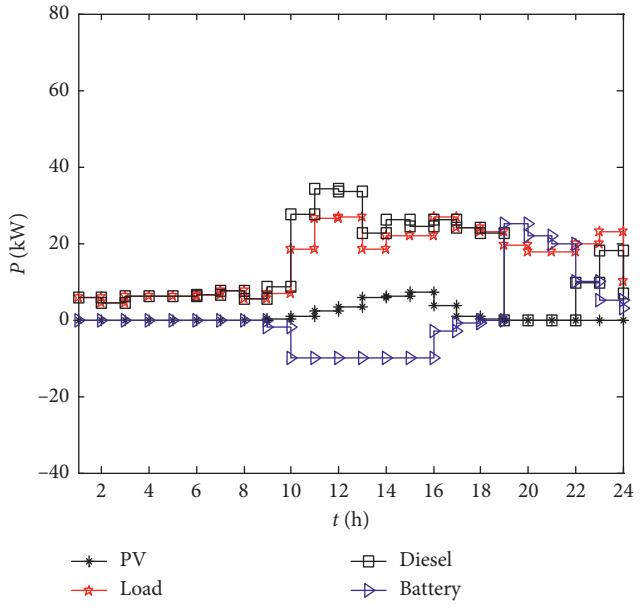

Figure 14: Distributed power and grid output power in Scenario 4.

6. Conclusion

In this paper, the modelling of a PV-diesel-battery MG system is accomplished with the precise economic and environmental parameters. The multiobjective Pareto optimization dispatch is constructed as a MOO problem. An advanced MPSO is developed on the basis of archive maintenance and Pareto selection. In this algorithm, the external archive helps to maintain the diversity of Pareto solutions. Four scenarios with various operation modes and illumination conditions are considered in the simulation experiment. The Pareto frontiers with two objects and three objects for the dispatch MOO problem are obtained by the proposed algorithm. The proposed algorithm shows the advantages on the nondominate Pareto frontiers and running time than the NSGA-II algorithm in benchmark tests and simulation experiment. The final trade-off solutions consisting of economic cost, environmental cost, and LOLP are obtained. It is proved that the model and algorithm researched in this paper are effective for the MOO dispatch of MG, which contain photovoltaic, diesel generator, Li ion battery, and electric vehicle charging points.

It is worthy pointing out that the stochastic process and power flow are not involved in this paper. In our future work, we will take the uncertainties of microgrids into account and introduce the stochastic process. The scenario-based stochastic optimal operation with load flow will be studied in the advance research.

Nomenclature

f_{pv}: PV array derating factor
P_{STC}: Maximum output power under standard test conditions (STCs)
$G(t)$: Actual sunlight intensity
G_{STC}: Sunlight intensity under the STC
k_{pv}: Power temperature coefficient
$T(t)$: Surface temperature of the PV array at time t
$T_{air}(t)$: Ambient temperature
T_{STC}: Surface temperature of the PV array under STC
T_{max}: Maximum temperature of the day
T_{min}: Minimum temperature of the day
t_p: Moment of average temperature
V_w: Current wind speed
C_{DE}: Fuel cost of diesel generator

$P_{DE}(t)$: Output power of diesel generator
a, b, c: Coefficients of fuel cost function
S_{load}, S_N: Capacity of load and service transformer
$SOC(t)$: Battery SOC at the time t
$I_e(t)$: Charging/discharging currents of battery at the time t
$P_{bat}(t)$: Output power of battery at the time t
η_{ch}: Battery charging efficiency
η_{dis}: Battery discharging efficiency
C_N: Nominal capacity of battery
E_0: Battery internal EMF
K_e, A, B: Fitting parameters of battery
C_{max}: Battery maximum capacity
Q_e: Battery discharged capacity
$f_s(x)$: Probability density function of daily EV traveling distance
μ_s: Mean of $f_s(x)$
σ_s^2: Variance of $f_s(x)$
S: Daily traveling distance of EV
W_{100}: Power consumption of an EV traveling 100 kilometres
P_c: Charging power of single EV
η_{C_EV}: EV charging efficiency
P_{EVi}: Charging power of an EV
$P_{EVload}(t)$: Total charge power of electric vehicles, $t = 1, 2, 3, \ldots, 24$
N_{EV}: Total number of adjustable electric vehicles
$F_k(X_i)$: Value of fitness function for the k_{th} subobjective with the particle X_i
$\alpha_i(t)$: Standard coefficients of the environmental value for the i_{th}-type pollutant
$\beta_i(t)$: Standard coefficients of the pollution penalty for the i_{th}-type pollutant
$Q_i(t)$: Emission of the i_{th} type of pollutant
N_P: Number of considered types of pollutant
$P_{tot}(t)$: Total power supply by the MG at time t
$P_{load}(t)$: Total load in the MG at time t
$P_{PV}(t)$: Output power of the PV at time t
$P_{gen}(t)$: Output power of the diesel generator at time t
$P_{bat}(t)$: Output power of the Li ion battery pack at time t
$P_i(t)$: Output power of the scheduled DG unit
$P_{i,min}$: The minimum output power of the scheduled DG unit
$P_{i,max}$: The maximum output power of the scheduled DG unit
$P_{grid,min}$: The minimum transmission power between MG and power grid
$P_{grid,max}$: The maximum transmission power between MG and power grid
SOC_{min}: The minimum allowable values of the SOC
SOC_{max}: The maximum allowable values of the SOC
β: Load rate
X_0: Solution vector
$\mathscr{P}_s$: Pareto optimal set
$\mathscr{P}_F$: Pareto optimal front
X_i: The i_{th} particle in MOPSO
V_i: Velocity of the i_{th} particle in MOPSO
$Pbest_i(t)$: The best position of the i_{th} particle
$Gbest_i(t)$: The best position of entire swarm
c_1, c_2: The acceleration constants
w: Inertia weight in MOPSO
w_{max}: The maximum value of w
w_{min}: The minimum value of w.
D_{ij}: Manhattan distance
M: Number of the objectives in AMOPSO
u_k: Constant and chosen to make all $u_k F_k$ close to each other
N_p: External archive
N_a: Size of current external archive
$hp(X_i)$: Number of particles whose global best position is X_i
$|F|$: Cardinality of the set F
S_p: Spacing matric
f_i: Membership function value of the i_{th} Pareto solution
f_{imin}: The minimum value of the i_{th} objective function
f_{imax}: The maximum value of the i_{th} objective function.

Data Availability

The data used to support the findings of this study are available from the corresponding author upon request.

Conflicts of Interest

The authors declare that they have no conflicts of interest.

Acknowledgments

This work was supported by the National Key R&D Program of China under 2016YFB0900400, National Natural Science Foundations (NNSF) of China under Grants 51507001, 51637001, and 61673001, and Doctoral research foundation of Anhui University under Grant J01001929.

References

[1] M. Elsied, A. Oukaour, T. Youssef, H. Gualous, and O. Mohammed, "An advanced real time energy management system for microgrids," *Energy*, vol. 114, pp. 742–752, 2016.
[2] X.-T. Feng and Z.-H. Zhang, "Coordinated control strategies with and without circulating current in unified power quality," *Journal of Power Electronics*, vol. 15, no. 5, pp. 1348–1357, 2015.
[3] M. S. Ballal, K. V. Bhadane, R. M. Moharil et al., "A control and protection model for the distributed generation and energy storage systems in microgrids," *Journal of Power Electronics*, vol. 16, no. 2, pp. 748–759, 2016.
[4] J. Sachs and O. Sawodny, "Multi-objective three stage design optimization for island microgrids," *Applied Energy*, vol. 165, pp. 789–800, 2016.
[5] H. Farzin, M. Fotuhi-Firuzabad, and M. Moeini-Aghtaie, "A stochastic multi-objective framework for optimal scheduling of energy storage systems in microgrids," *IEEE Transactions on Smart Grid*, vol. 8, no. 1, pp. 117–127, 2017.
[6] G. Ding, R. F. Gao, and B. Wu, "A communicationless PCC voltage compensation using an improved droop control scheme in islanding microgrids," *Journal of Power Electronics*, vol. 17, no. 1, pp. 294–304, 2017.

[7] X. T. Feng and Z. H. Zhang, "Unbalanced power sharing for islanded droop-controlled microgrids," *Journal of Power Electronics*, vol. 19, no. 1, pp. 234–243, 2019.

[8] M. Choobineh and S. Mohagheghi, "A multi-objective optimization framework for energy and asset management in an industrial Microgrid," *Journal of Cleaner Production*, vol. 139, pp. 1326–1338, 2016.

[9] A. A. Moghaddam, J. M. Guerrero, J. C. Vasquez, H. Monsef, and A. R. Kian, "Efficient energy management for a grid-tied residential MG," *IET Generation Transmission & Distribution*, vol. 11, no. 11, pp. 2752–2761, 2017.

[10] L. Igualada, C. Corchero, M. Cruz-Zambrano, and F.-J. Heredia, "Optimal energy management for a residential microgrid including a vehicle-to-grid system," *IEEE Transactions on Smart Grid*, vol. 5, no. 4, pp. 2163–2172, 2014.

[11] J. M. Houman, G. Ahmad, A. Loni et al., "A hybrid price-based demand response program for the residential microgrid," *Energy*, vol. 185, pp. 274–285, 2019.

[12] A. Maulik and D. Das, "Optimal operation of microgrid using four different optimization techniques," *Sustainable Energy Technologies and Assessments*, vol. 21, pp. 100–120, 2017.

[13] H. Nafisi, S. M. M. Agah, H. Askarian Abyaneh, and M. Abedi, "Two-stage optimization method for energy loss minimization in microgrid based on smart power management scheme of PHEVs," *IEEE Transactions on Smart Grid*, vol. 7, no. 3, pp. 1268–1276, 2016.

[14] K. Rahbar, J. Xu, and R. Zhang, "Real-time energy storage management for renewable integration in microgrid: an off-line optimization approach," *IEEE Transactions on Smart Grid*, vol. 6, no. 1, pp. 124–134, 2015.

[15] A. Mehdizadeh and N. Taghizadegan, "Robust optimisation approach for bidding strategy of renewable generation-based microgrid under demand side management," *IET Renewable Power Generation*, vol. 11, no. 11, pp. 1446–1455, 2017.

[16] Y. Huang, S. Mao, and R. M. Nelms, "Adaptive electricity scheduling in microgrids," *IEEE Transactions on Smart Grid*, vol. 5, no. 1, pp. 270–281, 2014.

[17] Y. Xu and X. Shen, "Optimal control based energy management of multiple energy storage systems in a microgrid," *IEEE Access*, vol. 6, pp. 32925–32934, 2018.

[18] X. Lu, K. Zhou, and S. Yang, "Multi-objective optimal dispatch of microgrid containing electric vehicles," *Journal of Cleaner Production*, vol. 165, pp. 1572–1581, 2017.

[19] M. Alsayed, M. Cacciato, G. Scarcella, and G. Scelba, "Multicriteria optimal sizing of photovoltaic-wind turbine grid connected systems," *IEEE Transactions on Energy Conversion*, vol. 28, no. 2, pp. 370–379, 2013.

[20] P. Li, D. Xu, Z. Zhou, W.-J. Lee, and B. Zhao, "Stochastic optimal operation of microgrid based on chaotic binary particle swarm optimization," *IEEE Transactions on Smart Grid*, vol. 7, no. 1, pp. 66–73, 2016.

[21] A. E. Moarref, M. Sedighizadeh, and M. Esmaili, "Multi-objective voltage and frequency regulation in autonomous microgrids using Pareto-based Big Bang-Big Crunch algorithm," *Control Engineering Practice*, vol. 55, pp. 56–68, 2016.

[22] M. A. Jrdehi, V. S. Tabar, R. Hemmati et al., "Multi objective stochastic MG scheduling incorporating dynamic voltage restorer," *International Journal of Electrical Power & Energy Systems*, vol. 93, pp. 316–327, 2017.

[23] A. A. Moghaddam, A. Seifi, T. Niknam, and M. R. Alizadeh Pahlavani, "Multi-objective operation management of a renewable MG (micro-grid) with back-up micro-turbine/fuel cell/battery hybrid power source," *Energy*, vol. 36, no. 11, pp. 6490–6507, 2011.

[24] A. A. Moghaddam, A. Seifi, and T. Niknam, "Multi-operation management of a typical micro-grids using particle swarm optimization: a comparative study," *Renewable and Sustainable Energy Reviews*, vol. 16, no. 2, pp. 1268–1281, 2012.

[25] N. Bazmohammadi, S. Bazmohammadi, and A. A. Moghaddam, "An efficient decision-making approach for optimal energy management of microgrids," in *Proceedings of the 2019 IEEE Milan PowerTech*, Milano, Italy, June 2019.

[26] M. B. Shadmand and R. S. Balog, "Multi-objective optimization and design of photovoltaic-wind hybrid system for community smart DC microgrid," *IEEE Transactions on Smart Grid*, vol. 5, no. 5, pp. 2635–2643, 2014.

[27] L. Guo, N. Wang, H. Lu, X. Li, and C. Wang, "Multi-objective optimal planning of the stand-alone microgrid system based on different benefit subjects," *Energy*, vol. 116, pp. 353–363, 2016.

[28] H. Haddadian and R. Noroozian, "Optimal operation of active distribution systems based on microgrid structure," *Renewable Energy*, vol. 104, pp. 197–210, 2017.

[29] H. R. Baghaee, M. Mirsalim, G. B. Gharehpetian et al., "Reliability/cost-based multi-objective Pareto optimal design of stand-alone wind/PV/FC generation microgrid system," *Energy*, vol. 115, pp. 1022–1041, 2016.

[30] G. Narges, K. Alibakhsh, T. Ashkan, L. Bahrami, and A. Maghami, "Optimizing a hybrid wind-PV-battery system using GA-PSO and MOPSO for reducing cost and increasing reliability," *Energy*, vol. 154, pp. 581–591, 2018.

[31] C. Wang, B. Hong, and L. Guo, "Dispatch strategies of PV-battery MG in different scenarios," *Power System Technology*, vol. 37, no. 7, pp. 1775–1782, 2013.

[32] M. Marzband, F. Azarinejadian, M. Savaghebi, E. Pouresmaeil, J. M. Guerrero, and G. Lightbody, "Smart transactive energy framework in grid-connected multiple home microgrids under independent and coalition operations," *Renewable Energy*, vol. 126, pp. 95–106, 2018.

[33] Z. Liu, Y. Chen, R. Zhuo et al., "Energy storage capacity optimization for autonomy MG considering CHP and EV scheduling," *Applied Energy*, vol. 210, pp. 1113–1125, 2018.

[34] J. Aghaei, M. A. Akbari, A. Roosta, and A. Baharvandi, "Multiobjective generation expansion planning considering power system adequacy," *Electric Power Systems Research*, vol. 102, pp. 8–19, 2013.

[35] M. A. Mirzaei, A. S. Yazdankhah, B. Mohammadi-Ivatloo, M. Marzband, M. Shafie-khah, and J. P. S. Catalão, "Stochastic network-constrained co-optimization of energy and reserve products in renewable energy integrated power and gas networks with energy storage system," *Journal of Cleaner Production*, vol. 223, pp. 747–758, 2019.

[36] P. Vikas and M. Rammohan, "Pareto dominance-based algorithms with ranking methods for many-objective optimization," *IEEE Access*, vol. 5, pp. 11043–11053, 2017.

[37] J. J. Ding, Q. J. Wang, Q. Zhang et al., "A hybrid particle swarm optimization- cuckoo search algorithm and its engineering applications," *Mathematical Problems in Engineering*, vol. 2019, Article ID 5213759, 12 pages, 2019.

[38] S. P. Wang, D. M. Zhao, and J. D. Yuan, "Application of NSGA-II Algorithm for fault diagnosis in power system," *Electric Power Systems Research*, vol. 175, Article ID 105893, 2019.

[39] G. Chen, L. Liu, P. Song, and Y. Du, "Chaotic improved PSO-based multi-objective optimization for minimization of power losses and L index in power systems," *Energy Conversion and Management*, vol. 86, no. 10, pp. 548–560, 2014.